https://doi.org/10.5194/bg-2020-295
Preprint. Discussion started: 2 September 2020

Biogeosciences Discussions

Dynamics of the Deep Chlorophyll Maximum in the Black Sea as depicted by BGC-Argo floats

Florian Ricour[1,2,*], Arthur Capet[1,*], Fabrizio D'Ortenzio[2], Bruno Delille[1], and Marilaure Grégoire[1]

[1]Freshwater and OCeanic science Unit of reSearch (FOCUS), University of Liege, Belgium
[2]Laboratoire d'Océanographie de Villefranche, Sorbonne Universités, Villefranche-sur-Mer, France
[*]AC and FR equally contributed to the production of this paper

Correspondence: Arthur Capet (acapet@uliege.be)

Abstract. The Deep Chlorophyll Maximum (DCM) is a well known feature of the global ocean. However, its description and the study of its formation are a challenge, especially in the peculiar Black Sea environment. The retrieval of Chlorophyll a (Chla) from fluorescence (Fluo) profiles recorded by Biogeochemical-Argo (BGC-Argo) floats is not trivial in the Black Sea, due to the very high content of Colored Dissolved Organic Matter (CDOM) which contributes to the fluorescence signal and produces an apparent increase of the Chla concentration with depth.

Here we revised Fluo correction protocols for the Black Sea context using co-located in-situ High-Performance Liquid Chromatography (HPLC) and BGC-Argo measurements. The processed set of Argo Chla data (2014–2019) is then used to provide a systematic description of the seasonal DCM dynamics in the Black Sea, and to explore different hypotheses concerning the mechanisms underlying its development.

Our results show that the corrections applied to Chla profiles are consistent with HPLC data. In the Black Sea, the DCM is initiated in March, throughout the basin, at a pycnal level set by the previous winter mixed layer. The DCM then remains attached to this particular layer until the end of September. The spatial homogeneity of this feature suggests a self-sustaining DCM structure, locally influencing environmental conditions rather than adapting instantaneously to external factors.

In summer, the DCM concentrates around 50 to 65% of the total chlorophyll content around a depth of 30 m, where light conditions ranged from 0.5 to 4.5% of surface incoming irradiance.

In October, as the DCM structure is gradually eroded, a longitudinal gradient appears in the DCM pycnal depth, indicating that autumnal mixing induces a relocation of the DCM which is this time driven by regional factors, such as nutrients lateral loads and turbidity.

1 Introduction

The Black Sea is a semi-enclosed basin receiving discharges from a catchment area covering European and Asian continents over a surface more than four times larger than that of the Black Sea. The intrusion of saline (salinity $\approx$ 36) Mediterranean

https://doi.org/10.5194/bg-2020-295
Preprint. Discussion started: 2 September 2020


Biogeosciences Discussions Open Access EGU

waters into the Black Sea and the large riverine inflow have created a permanent halocline, resulting in an extremely stable vertical stratification. Waters below the main pycnocline ($\approx$ 100-150 m) are ventilated by cold water formation and convection (Ivanov et al., 1997; Stanev et al., 2003; Miladinova et al., 2018), intrusion of the Mediterranean inflow and subsequent entrainment of surface and intermediate waters (Özsoy et al., 2001; Falina et al., 2017), as well as mesoscale activity along the shelf break (Ostrovskii and Zatsepin, 2016). However, those ventilation mechanisms are not sufficient to ventilate deep waters and the residence time of Black Sea water masses increases from a few years in the layer of the main pycnocline to several hundred years for the deep sea (Murray et al., 1991). Therefore, almost 90% of the Black Sea's volume is devoid of oxygen, contains large amounts of reduced elements (e.g. hydrogen sulphide, ammonium) and is only inhabited by organisms that have developed anaerobic respiration pathways. Those conditions set a very specific environment, which affects many aspects of the marine biogeochemical cycles. In particular, the absence of oxygen causes the degradation of detrital matter to be less efficient (Claustre et al., 2008), resulting in the accumulation of large quantities of Coloured Dissolved Organic Matter (CDOM), much larger than in the Mediterranea Sea (Organelli et al., 2014) and in the global ocean (Nelson and Siegel, 2013).

If the relationship between the physical vertical structure and the profiles of chemical elements have been extensively investigated (e.g. Tugrul et al., 1992; Konovalov and Murray, 2001), the imprint of the vertical density structure on living organisms at basin scale and, in particular, primary producers is by far less addressed.

Yunev et al. (2005) analysed the subsurface chlorophyll peak in summer over the period 1964-1992 addressing a potential shift due to eutrophication and climate change. More specifically, based on the analysis of 352 profiles (mostly from the Black Sea NATO TU Database) collected in the deep sea from March to November, the authors concluded that the depth of the Deep Chlorophyll Maximum (DCM) and its chlorophyll content can be considered as spatially homogeneous and highlighted a vertical decoupling between the chlorophyll subsurface peak and nitrate maximum. The authors highlighted the importance of considering the mechanisms of the DCM dynamics to understand the response of primary production in the central Black Sea to the important eutrophication period that affected the Black Sea in the 1970s and 1980s.

In addition, Finenko et al. (2005) showed that in the deep part of the basin, uniform chlorophyll a (Chla) profiles with high concentrations were mostly observed between December and March when the winter mixing is strong with the absence of a thermocline. Then, by the end of spring as the thermocline forms, the majority of Chla profiles showed a subsurface chlorophyll peak, highly variable in depth, that was stable until the end of summer. A new transition to uniform Chla profiles, due to the weakening of the thermal stratification and the strengthening of the vertical mixing occurred later in November.

More recently, the composition and phenology of planktonic blooms have been investigated on the basis of in-situ sampling in concert with contemporaneous remote-sensing and autonomous profiler data, therefore focusing on local scales and addressing mechanisms triggering surface blooms. For instance, the winter-spring bloom phenology has been investigated using Chla derived from satellite data (Mikaelyan et al., 2017b, a) while in Mikaelyan et al. (2018), in-situ data are used to identify and explain species succession. These works highlighted a clear differentiation of planktonic community composition in surface and sub-surface layers (Mikaelyan et al., 2018, 2020) and the importance of environmental factors such as surface

https://doi.org/10.5194/bg-2020-295
Preprint. Discussion started: 2 September 2020

winds (Mikaelyan et al., 2017b) and mesoscale vertical dynamics (Mikaelyan et al., 2020) in triggering local surface blooms in autumn. The winter-spring bloom dynamics, and its interannual variations in particular, have been depicted in details and used to propose the Pulsing Bloom hypothesis (Mikaelyan et al., 2017a), an extension of the general Critical Depth hypothesis and its derivatives (Sverdrup, 1953; Huisman et al., 1999; Chiswell et al., 2015), that applies to highly stratified waters.

Basin scale and seasonal perspective have often been adopted in studies addressing surface Chla dynamics on the basis of remote-sensing observations, exploiting the synoptic nature of those datasets. These studies generally depict a clear seasonal cycle in the central Black Sea, with maximal surface Chla concentrations observed during winter-spring and autumn blooms (e.g. Kopelevich et al., 2002; Finenko et al., 2014), and minimal concentrations in summer. However, the extent to which this seasonal cycle is representative of vertically integrated Chla content is challenged as soon as vertical profiles are considered (Finenko et al., 2005).

Today, the advent of autonomous profilers allows an even seasonal sampling and permits to adopt this annual and basin-wide perspective to study the dynamics of the vertical chlorophyll distribution, and especially the DCM, which has not been clearly investigated *per se* in the Black Sea. The DCM, also known as the Subsurface Chlorophyll Maximum (Cullen, 2015) is a common widespread feature of the world's ocean characterized by a subsurface layer of maximum Chla concentration. This Chla subsurface maximum can correspond either to a maximum in phytoplankton biomass (Varela et al., 1992; Estrada et al., 1993; Beckmann and Hense, 2007; Mignot et al., 2014) or to a change in the cellular Chla content resulting from a physiological adaptation, known as photo-acclimatation. Therefore, the DCM is not necessarily associated to a peak in biomass (Fennel and Boss, 2003) and can either be an enhancing mechanism for species adapted to low light intensities (Fennel and Boss, 2003; Dubinsky and Stambler, 2009) or a protective mechanism at high irradiance intensities near the water surface (Marra, 1997; Xing et al., 2012). Although it has been studied for more than 60 years (Anderson, 1969; Cullen, 1982; Furuya, 1990; Parslow et al., 2001; Huisman et al., 2006; Ardyna et al., 2013), the mechanisms of formation and maintenance of DCM are still debated and are reviewed in Cullen (2015). When the DCM is associated to a peak in biomass, the reasons evoked to explain its occurrence mainly refer to instantaneous factors, such as maximum growth conditions resulting from a compromise between light and nutrients limitations, aggregation at a particular density gradient (Richardson and Cullen, 1995) or reduced grazing (Macedo et al., 2000).

More recently however, Navarro and Ruiz (2013) proposed another explanation arguing that the DCM emerges from the bloom history prolonging the winter bloom at a density corresponding to that of the winter mixed layer. The DCM would act as a self-preserving biological structure that maintains over the year at its density by preventing the nutrient flux from below to reach overlying waters while limiting the growth in the underlying waters through shading effect. This theory advocates that the DCM can not be solely explained by instantaneous conditions but rather results from a hysteresis of the water mass. It can explain why the analysis of chlorophyll profiles in the global temperate ocean and in the Mediterranean Sea evidences that if the depth of the DCM may be highly variable, its density of occurrence remains quite unchanged (Yilmaz et al., 1994; Ediger and Yilmaz, 1996; Navarro and Ruiz, 2013).

The peculiarities of the open Black Sea environment, i.e. its strong and stable stratification, and the relatively low water transparency (Kara et al., 2005), makes it an interesting site to study the DCM dynamics at basin scale.

https://doi.org/10.5194/bg-2020-295
Preprint. Discussion started: 2 September 2020


Biogeosciences Discussions Open Access EGU

Estimation of chlorophyll concentrations from the signal produced by fluorometers requires the use of empirical equations. Indeed, the relationship between Chla and the fluorescence (Fluo) can be altered due to, on one hand, the variability in the phytoplankton species composition and physiological response to environmental conditions (e.g. light, nutrients). Therefore, for a given chlorophyll concentration, the amount of emitted fluorescence may differ (Claustre et al., 2009; Xing et al., 2011, 2012). On the other hand, the presence of high concentrations of CDOM and particulate coloured detrital material (e.g. phaeopigments) can also contribute to the Fluo signal emitted in the bandwidth of Chla fluorometers (Cullen, 1982; Proctor and Roesler, 2010). This last point is particularly critical in an anoxic environment like the Black Sea (Coble et al., 1991) where a quasi-linear increase of Chla concentrations with depth has been observed (Xing et al., 2017) and can be referred to in the litterature as the deep sea red fluorescence (e.g. Röttgers and Koch, 2012).

In this study, we used $\approx$ 1000 Chla profiles delivered from 5 Biogeochemical-Argo (BGC-Argo) floats deployed in the Black Sea for the period 2014-2019 in order to investigate the vertical structure of the bloom and, in particular, the process of formation and maintenance of the DCM. To this aim, we derived local parameters to apply the correction method of Xing et al. (2017) for inferring Chla content from Fluo data and we validated this calibration using High-Performance Liquid Chromatography (HPLC) measurements. This extensive and validated dataset is then exploited to identify general characteristics of the vertical structure of Chla distribution and explore their seasonal and spatial variability using both depth and density vertical scales, in order to describe the morphology, seasonal dynamics and relevance of DCM in the Black Sea, in particular in regards to synoptic surface Chla dynamics that is depicted by remote-sensing observations.

2 Material and methods

2.1 Dataset preparation

Data from 5 BGC-Argo floats (WMO 6900807, 6901866, 6903240, 7900591 and 7900592) were downloaded from the Coriolis data center (ftp://ftp.ifremer.fr/ifremer/argo/dac/coriolis/) for a six-year period (2014-2019), i.e. 1400 vertical profiles. All floats have a Chla fluorometer (excitation at 470 nm; emission at 695 nm) and a particle backscattering sensor (BBP) at 700 nm while only floats 6900807, 6901866 and 6903240 carry a WET Labs ECO FLBBCD that involves, in addition to a Chla fluorometer and a BBP sensor, a CDOM fluorometer (excitation at 370 nm; emission at 460 nm). Photosynthetic available radiation (PAR) data were provided by a Satlantic OCR-504 Multispectral Radiometer for all floats but one (6900807). Additionally, T and S data were obtained from a CTD Seabird model 41CP for all floats.

First, descending profiles were removed (398 profiles, the majority of them was empty for the float 6903240) because the time interval between ascending and descending profiles was too short (hours) to observe significant differences in the Chla distribution between these two profiles. Then, 18 profiles were removed for consistency and automatization of the data processing: missing metadata (latitude and/or longitude), no data above 5 m, a bottom depth too shallow (i.e. less than 40 m) or because pressure data were wrong (i.e. "stuck" profiles). Finally, Chla profiles were firstly quality controlled by removing data

https://doi.org/10.5194/bg-2020-295
Preprint. Discussion started: 2 September 2020

points considered as bad data, i.e. Quality Control (QC) = 4 (Argo Data Management Team, 2019; Schmechtig et al., 2018) while data with a QC = 3 (i.e. probably bad data) were retained because most of the time this flagging is due to the increase of measured Fluo with depth, a common feature in the Black Sea. Indeed, the presence of large amounts of CDOM and poorly degraded Chla pigments due to anoxic conditions lead to an increase of the Chla signal with depth, resulting in an in-situ estimated Chla dark signal (Fluo value measured by the fluorometer in the absence of Chla) significantly different from its factory calibration (Schmechtig et al., 2018). On the other hand, BBP profiles were quality controlled (removing 4 additional profiles with QCs 3 and 4), whereas CDOM profiles were simply extracted (CDOM has no quality control yet, i.e. QC = 0). Finally, the selected data (980 profiles of Chla, BBP and CDOM) were smoothed with a 5-point moving median filter along the vertical dimension.

PAR data were quality controlled using the method described in Organelli et al. (2016). T and S data with a QC = 1 or 2 (i.e. respectively good and probably good data) as in Wong et al. (2018) were used to compute the σ_θ profiles referenced to the sea surface and defined by the Thermodynamic Equation Of Seawater of 2010 (IOC, SCOR and IAPSO, 2010). In the Black Sea, the Mixed Layer Depth (MLD) is usually defined as the depth at which the density is greater than 0.125 $\mathrm{kg\,m^{-3}}$ compared to the surface density (i.e. 3 m) as proposed by Kara et al. (2009). Unfortunately, T and S data near the surface were often flagged as potential bad data and thus the MLD was determined by the depth at which the density exceeded by 0.03 $\mathrm{kg\,m^{-3}}$ the 10-m density anomaly as proposed in de Boyer Montégut et al. (2004). 3 profiles were removed because their MLD could not be determined.

2.2 Retrieval of Chla from fluorometers

The retrieval of Chla data from Fluo involves three main steps: the application of a regional bias correction due to fluorometer calibration issue, the correction of the deep sea red fluorescence due to the presence of high amounts of CDOM, affecting the signal perceived by Chla fluorometers and the correction for Non-Photochemical Quenching (NPQ) in the surface waters.

First, due to a systematic bias in Chla data from WET Labs fluorometers, we applied a correction factor of 0.65 to all Chla profiles, following the recommendations of Roesler et al. (2017) for the Black Sea.

Second, as already noted by Xing et al. (2017), the Fluo signal measured by BGC-Argo floats in the Black Sea is linearly increasing with depth below 100 m up to 1000 m (parking depth of the float) instead of presenting the typical constant offset associated to the sensor bias (from factory calibration) that can be corrected using the so-called deep-offset correction (Schmechtig et al., 2018). The profile of this deep sea red fluorescence is very similar to that of CDOM, as illustrated in Fig. 2. Therefore, the Chla-Fluo equation needs to be adapted for the presence of CDOM in oxygen deficient environments. Here we used the method proposed by Xing et al. (2017), referred to as the FDOM-based method, that removes from the Chla fluorescence signal the contribution of CDOM, assumed to be proportional to the amount of CDOM (Appendix A). The FDOM-based method was applied on the three floats carrying a CDOM fluorometer whereas the minimum-offset method correction described in Xing et al. (2017) was used on the other two. The latter consists in subtracting from each profile the minimum value of Chla found at depth (i.e. the depth at which Chla is assumed to be zero) and sets the profile to zero below that depth.

https://doi.org/10.5194/bg-2020-295
Preprint. Discussion started: 2 September 2020

Finally, all daytime profile were corrected for NPQ, a protective mechanism triggered at cellular level in high light intensities, which induces a reduction of the fluorescence signal for a same amount of Chla. Daytime and nighttime profiles were determined based on the *suncalc* package (RStudio Team, 2016) which provides a tool to obtain the sun position for a given location, hence allowing the computation of the local sunset and sunrise. We assume that NPQ does not affect nighttime profiles because these profiles are collected a few hours after (before) the sunset (sunrise). Daytime profiles were corrected for NPQ by extrapolating the maximum Chla value observed over 90% of the MLD up to the surface (Schmechtig et al., 2018). Eventually, we set to zero all negative Chla concentration. They vary from $\approx 10^{-7}$ to 10^{-2} $\mathrm{mg\,m^{-3}}$ and represent $\approx 28\%$ of all Chla observations. However, those negative concentrations are firstly observed below 80 m on average and therefore appear between 80 m and the bottom of the profile ($\approx$ 1000 m) where we assume, based on HPLC data, that there is no more Chla.

2.3 Data processing

In order to discriminate profiles depicting a DCM signature, all Chla profiles were fitted to 5 specific mathematical forms which are considered to represent the diversity of Chla vertical profiles (Mignot et al., 2011; Carranza et al., 2018): a sigmoid ("S"), an exponential ("E"), a Gaussian ("G"), a combination of a Gaussian with a sigmoid ("GS") and a combination of a Gaussian with an exponential ("GE") (Fig. 1, Appendix B). The Gaussian was modified to take into account the possible asymmetry of the Chla vertical profile with higher values at the surface rather than at depth as in Mignot et al. (2011). The selected 977 profiles were fitted using a nonlinear square fit function applying the Levenberg-Marquardt algorithm (Moré, 1978) using the R package *minpack.lm*. For each fit, an adjusted coefficient of determination, R^2_{adj}, was computed to take into account the number of parameters involved in the mathematical forms and thus avoid over-fitting. As in Mignot et al. (2011), profiles for which the R^2_{adj} was below 0.9 for all forms were classified as "Others" (27 profiles). The remaining profiles (950) were classified according to their best fit.

2.4 Chla sampling and float deployment

In view of validating the Chla-Fluo relationship in the Black Sea, a new BGC-Argo float (WMO 6903240) equipped with both Chla and CDOM fluorometers was deployed in the western Black Sea on the 29th of March 2018. Conjointly at the site of deployment, water samples were collected for Chla determination in the lab. This sampling took place on board the RV *Akademik* (Institute of Oceanology – Bulgarian Academy of Sciences) at a station localized at 43°10'N and 29°E. Seawater samples were obtained using a CTD carousel equipped with twelve 5-L Niskin bottles. Samples were taken at 12 different depths between 1000 m and the surface, and were considered to be co-located in time and space with the float first profiles. After that, seawater samples were vacuum filtered through 47 mm diameter Whatman GF/F glass fibre filters (0.7 $\mu\mathrm{m}$ pore size). No bloom was present during that period at this location. Filtered volumes varied between 4 L near the surface and approximately 5 L between 100 m and 1000 m. After filtration, filters were immediately stored in liquid nitrogen and then at -80°C until HPLC analyses at the Villefranche Oceanographic Laboratory. These analyses were performed using the procedure from Ras et al. (2008) for the determination of Chla concentrations and other pigments. The first deep Chla profile taken by the

https://doi.org/10.5194/bg-2020-295
Preprint. Discussion started: 2 September 2020


Biogeosciences Discussions Open Access EGU

float after deployment (during the descent) was used to retrieve Chla using the FDOM correction and compared with HPLC data.

2.5 Profile diagnostics

To characterize the Chla vertical distribution and its environmental context we consider the following diagnostics.

- z_{low} locates the deepest penetration of Chla ($> 0.01\ \mathrm{mg\,m^{-3}}$).
- $z_{50,bottom}$ and $z_{50,up}$ were derived as boundaries to the bulk of the chlorophyll content. Both were obtained by assessing the depth needed to obtain 75% of total Chla content by vertical integration, going downward from surface ($z_{50,bottom}$) and upward from 200 m ($z_{50,up}$). These boundaries thus locate the depth interval containing 50% of the Chla content (hereafter referred to as the bulk of Chla content or the Chla bulk).
- z_{DCM} indicates the depth of the DCM.
- z_{MLD} indicates the depth of the MLD.
- $z_{\mathrm{PAR}1\%}$ indicates the depth where in-situ PAR reaches 1% of its surface values.

The pycnal depths of diagnostics presented above are noted similarly using σ instead of z, and obtained from interpolation of potential density anomalies at sampling depths.

2.6 Backscattering data and normalization

In order to evaluate the correspondence between chlorophyll and phytoplankton cells, we consider BBP data.

This is the best proxy that can be obtained from the current Black Sea BGC-Argo dataset, although the complexity and variability of the Black Sea optical properties prohibit the establishment of a strict relationship between BBP and the presence of phytoplanktonic cells.

To establish an uniform context, allowing to proceed with this comparison while overcoming the variability in vertical distribution and absolute concentration values, the Chla, BBP and depth values are normalized for this case as follows:

$$z_{norm} = \frac{z - z_{MLD}}{z_{DCM} - z_{MLD}} \tag{1}$$

$$Chla_{norm} = \frac{Chla}{Chla_{DCM}} \tag{2}$$

$$BBP_{norm} = \frac{BBP}{BBP_{max}}, \tag{3}$$

https://doi.org/10.5194/bg-2020-295
Preprint. Discussion started: 2 September 2020

where BBP_{max} is the maximum BBP value evaluated for each individual profiles between the surface and 1.5 times z_{DCM}. The latter vertical restriction is considered to avoid the peak in BBP that is typically visible in the vicinity of the anoxic interface and is related to bacterial activity (Karabashev, 1995).

3 Results

3.1 Validation of the FDOM-based method in the Black Sea

In this section, HPLC data taken at deployment will be compared with successive levels of correction on Chla data: 1) No correction (raw data), 2) Application of the correction factor of Roesler et al. (2017) for the Black Sea on raw data, 3) FDOM-based correction of Xing et al. (2017) and 4) NPQ correction, in order to validate the global correction of Chla profiles in the Black Sea.

Firstly, HPLC data evidence the absence of Chla below a depth of 200 m (< 0.01 $\mathrm{mg\,m^{-3}}$, ranging from 0.002 to 0.004 $\mathrm{mg\,m^{-3}}$). The increase in the fluorescence signal (Fig. 2) that characterizes Black Sea Chla profiles, is thus not associated to Chla but more likely results from the presence of high levels of CDOM as suggested by Xing et al. (2017).

Then, a regional correction factor of 0.65 following the recommendation of Roesler et al. (2017) was applied on all data (results in Table 1) before using the FDOM-based correction. The shape of the Chla profile after the FDOM correction in the surface layer is questionable. Based on HPLC data, it seems that it displays a Sigmoid shape. However, based on Chla not corrected for NPQ, it is qualified as a Gaussian-exponential with a $\frac{Chla_{DCM}}{Chla_{surface}}$ ratio of ≈ 1.8. Corrected for NPQ, the aforementioned algorithm qualifies it as a Gaussian-sigmoid but rejects it due to its ratio $Chla_{DCM}/Chla_{surface}$ of 1. This discrepancy highlights the importance of NPQ correction for daytime Chla profiles. Although, a denser vertical sampling for the HPLC acquisition would have been needed to demonstrate the total absence of a subsurface chlorophyll maximum. In deeper waters, not affected by NPQ, the Chla minimum measured by the float (on the red curve, i.e. no correction) is located at 98.5 m (0.102 $\mathrm{mg\,m^{-3}}$) while the minimum non negligible value from discrete water samples (HPLC) is located at 140 m (0.012 $\mathrm{mg\,m^{-3}}$). Below that depth, Chla concentrations can be considered as zero. In the deep layer (i.e. below the Chla minimum, see also Fig 2), the RMSE[1] between Chla estimations obtained by HPLC (observations) and Chla retrieved from the ROESLER+FDOM Chla corrected profile (modeled values) is equal to 0.01 $\mathrm{mg\,m^{-3}}$ while the RMSE for raw data is 0.1985 $\mathrm{mg\,m^{-3}}$. In the surface layer, the RMSE is equal to 0.13, 0.05 and 0.20 $\mathrm{mg\,m^{-3}}$ for the ROESLER+FDOM, the ROESLER+FDOM+NPQ and the uncorrected profiles, respectively. Therefore, we assume that the ROESLER+FDOM+NPQ correction is a consistent approach for Chla profiles in the Black Sea, and we use the notation $Chla$ to denote $F_{Chla,ROESLER+FDOM+NPQ}$ data for the rest of the manuscript.

[1] Root Mean Squared Error, $\mathrm{RMSE} = \sqrt{\frac{\sum_{n=1}^{N}(obs_n - mod_n)^2}{N}}$ where obs are observations, mod are modeled values and N is the number of points.

https://doi.org/10.5194/bg-2020-295
Preprint. Discussion started: 2 September 2020

Biogeosciences Discussions Open Access EGU

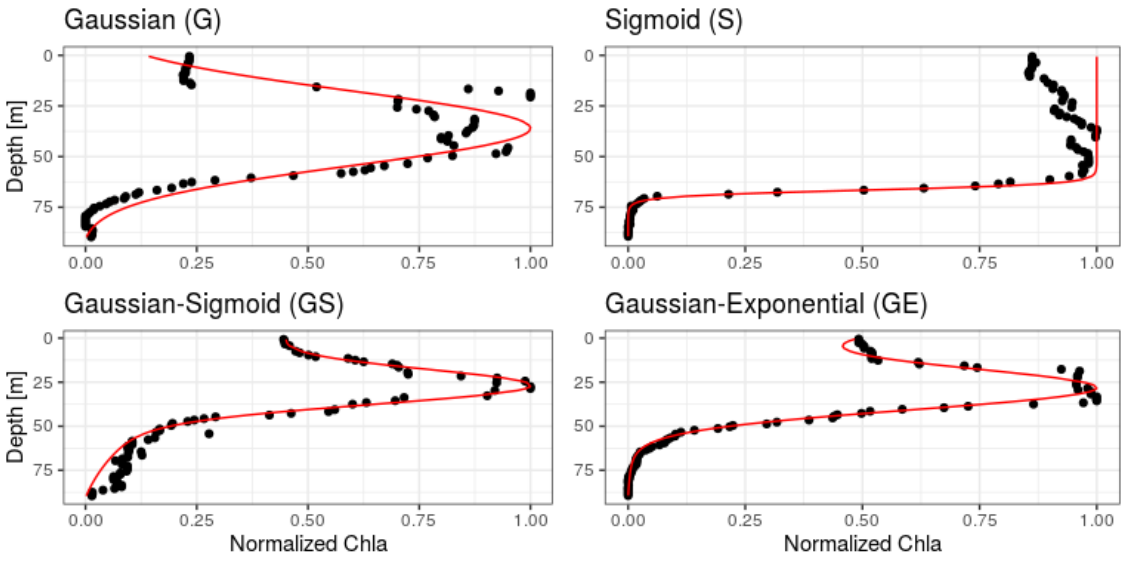

Figure 1. Examples of Chla profiles matching the 4 observed analytical functions

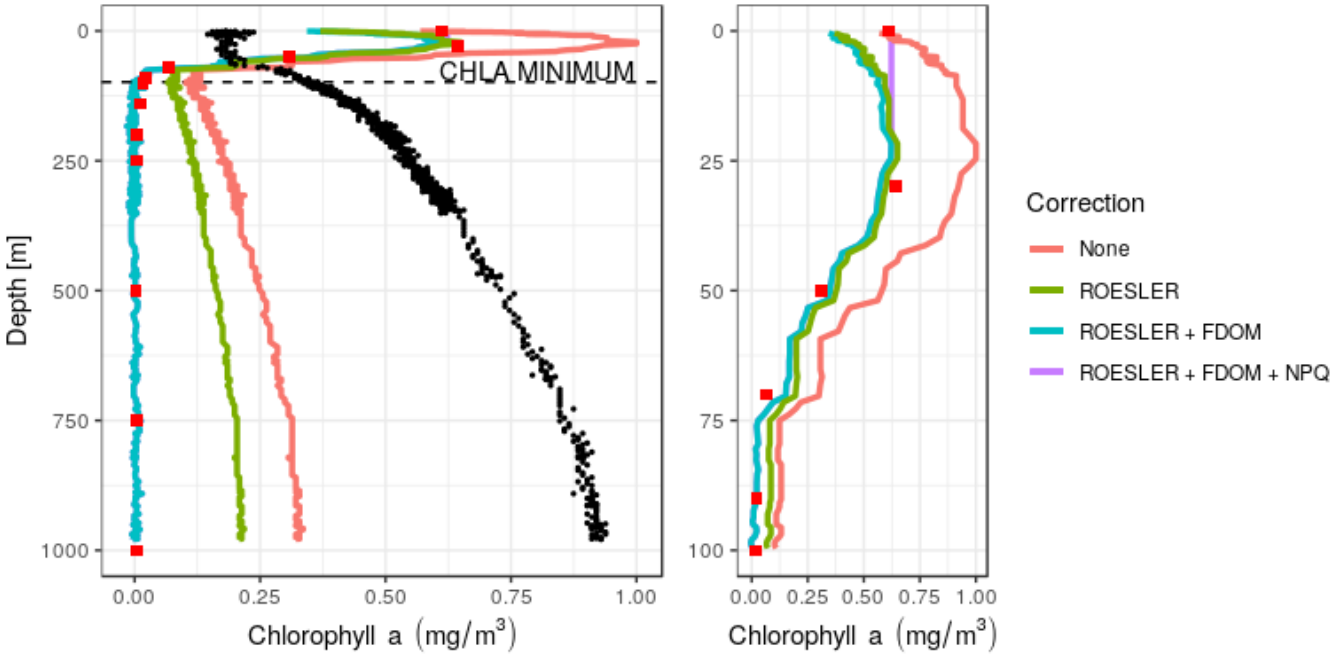

Figure 2. Vertical Chla profiles obtained at the deployment of the float 6903240 on the 29/03/2018 at 49°10'N and 29°E, using different levels of correction. HPLC data are depicted in red squares and CDOM (in ppb/10) in black dots. Right panel: zoom in the surface layer.

https://doi.org/10.5194/bg-2020-295
Preprint. Discussion started: 2 September 2020

	Deep Layer	Surface Layer	Entire profile
No correction (raw data)	0.199	0.208	0.215
ROESLER	0.127	0.130	0.137
ROESLER+FDOM	0.010	0.131	0.085
ROESLER+FDOM+NPQ	0.010	0.053	0.035

Table 1. RMSE ($\mathrm{mg\,m^{-3}}$) comparison between HPLC measurements and Chla retrieved from Fluo using different levels of correction.

3.2 Categories of Chla profiles

Chla profiles are firstly categorized according to the best-fitting analytical form (Fig. 3). Despite the use of a R^2_{adj} metric, it seems that the plasticity of the Gaussian-sigmoid formulation provides a best fit in most cases. The best-fitting form can therefore not be used as a single criterion to discriminate DCM and non-DCM profiles, and individual profiles are further requested to have a Chla concentration at the DCM that is at least a third higher than at the surface to be tagged as DCM profiles. This criterion was chosen based on visual inspection, to filter out profiles wrongly tagged as DCM due to signal fluctuations near the surface. Non-DCM profiles dominate from November to March, while a clear DCM dynamics sets in from April to October. A complication arises in this DCM seasonal sequence when profiles categorized as "Others" are counted as non-DCMs (Fig. 3). Those profiles most often consist in double peaks, which explain their rejection based on R^2_{adj}. Yet, all series of "Other" profiles for each individual float are systematically preceded and followed by DCM forms. In the following, "Others" are thus considered as local perturbations of DCM structures (e.g. Mikaelyan et al., 2020) and included among DCM profiles.

The non-DCM season is largely dominated by Gaussian-sigmoid forms. Pure exponential profiles are never observed. The pure sigmoid profiles, which denote a well-homogenized planktonic biomass in the surface layer, are observed from October to April with a clear peak in December/January, in consistence with the known seasonality of the MLD in the Black Sea (e.g. Capet et al., 2014).

The DCM season opens mainly with Gaussian-sigmoid profiles. Later, Gaussian-exponential and finally simple Gaussian profiles are observed, which denote a successive depletion of the surface Chla content (Fig. 3).

No meaningful spatial structuring of the DCM dynamics components can be evidenced at first glance (Fig. 4) and it appears that the deep basin can be considered as homogeneous regarding to the beginning and the end of the DCM season, as far as the current sampling allows to perceive.

3.2.1 Depth and density horizons

Here we present the seasonal evolution of diagnostics (cf. Sect. 2.5) extracted from Chla profiles and their environmental context, using both depth and density vertical scales, and referred to as depth-diagnostics and density-diagnostics, respectively. DCM-specific diagnostics are not considered from November to March.

https://doi.org/10.5194/bg-2020-295
Preprint. Discussion started: 2 September 2020


Biogeosciences Discussions Open Access EGU

In winter, the deep MLD bounds the productive area, and a clear coincidence is visible between $z_{50,bottom}$ and z_{MLD} at $\sim$ 30-40 m in December, January and February (Fig. 5). Chla in this period penetrates to depths of 70 m. A large spread, illustrated by the interquartile ranges in Fig. 5, is observed for most depth-diagnostics during this period.

As stratification establishes progressively in March, z_{MLD} gets shallower and the bulk of Chla content penetrates slightly deeper, with a progressive appearance of DCM profiles (Fig. 3). The DCM is first formed at the lower boundary, $z_{50,bottom}$, around 40 m and remains in the lower part of the Chla bulk until June. During this transition period, z_{low} extends downward to 80 m.

The vertical structure remains stable during the month of June, July and August. For this period, the DCM depth is sensibly shallower (30 m) than during the formation months and presents a large spread between 12 and 50 m. The median value of z_{DCM} is now clearly distinguished from that of $z_{50,bottom}$. Until August, the bulk Chla area slightly narrows around z_{DCM} and remains located well below z_{MLD}.

In September and October, the thermocline starts to weaken. $z_{50,top}$, $z_{50,bottom}$ and z_{low} migrate upwards. As z_{DCM} upward migration is slower, it is rejoined by $z_{50,bottom}$. The spread of z_{DCM} in the end of the DCM season is narrow, compared to the rest of the year, and spans between 17 and 40 m.

While $z_{\mathrm{PAR}1\%}$ is homogeneously (low spread) located around 30 m in December and January, its spread expands for the rest of the year, denoting a more important spatial variability. $z_{\mathrm{PAR}1\%}$ is located slightly above $z_{50,bottom}$ and close to z_{DCM} in the first part of the year, but seems to penetrate below z_{DCM} and to reach $z_{50,bottom}$ content from August onward.

Exploring the seasonal evolution of the above diagnostics on a density scale provides another point of view which is better adapted to depict processes driven by diffusive transport along isopycnals.

By definition, σ_{MLD} corresponds to the density in the MLD which varies between 10 and 60 m in winter (Fig. 6). It appears that the highest winter σ_{MLD} sets the lower pycnal depth of the bulk of Chla content, $\sigma_{50,bottom}$, which remains stable from February to September.

Again, the DCM first forms at $\sigma_{50,bottom}$, and then settles in slightly lighter layers until October. The spread of σ_{DCM} is relatively narrow during the DCM season but expands in September and October. The spread of $\sigma_{50,up}$ also largely increases in September, while that of $\sigma_{50,bottom}$ extends later in October. The σ-layer of deepest Chla records is quite stable along the season and coincides with the nitracline level, located at 15.5 $\mathrm{kg\,m^{-3}}$ by Konovalov et al. (2006).

Interestingly, $\sigma_{\mathrm{PAR}1\%}$ depicts a quite narrow spread during the main DCM period (June, July, August), while it bears an important spread on the depth scale (Fig. 5).

3.3 Chla concentrations and integrated content

Here, we consider seasonal variations in Chla concentrations at the surface, at the DCM and integrated over the vertical, as well as the vertical distribution of this integrated Chla content.

The average Chla concentration is defined to represent the integrated Chla content. In order to obtain units of volumetric concentration ($\mathrm{mg\,m^{-3}}$), the integrated Chla content is scaled by a constant depth of 40 m, chosen as the mean of $z_{50,bottom}$.

https://doi.org/10.5194/bg-2020-295
Preprint. Discussion started: 2 September 2020

Ranging between 0.5 and 2 $\mathrm{mg\,m^{-3}}$ (i.e. 20 and 80 $\mathrm{mg\,m^{-2}}$), the total Chla content only presents weak seasonal variations with a maximum in March (Fig. 7). The spread of this integrated content is rather constant along the year.

Surface chlorophyll concentration, instead, has a marked seasonal variability and decreases by a factor of two to reach 0.35 $\mathrm{mg\,m^{-3}}$ from April to September, while Chla concentrations at the DCM is generally close to 1 $\mathrm{mg\,m^{-3}}$ in this period and reaches mean values above 1.5 $\mathrm{mg\,m^{-3}}$ in August.

To summarize the above descriptions, roughly 80% of the chlorophyll content is contained within the MLD in winter, while this ratio falls to 10% during the DCM season (Fig. 8). In summer, about 50% of the integrated content can be found within a 10 m layer surrounding the DCM, a value that peaks in August and reaches 80% in some cases.

3.4 Normalized chlorophyll and backscattering profiles

We analyze here the normalized Chla and BBP values (Sect. 2.6) computed for DCM profiles, and in particular the eventual correspondence between local maxima at z_{DCM}, in order to characterize the nature of the DCM.

The shapes of normalized Chla profiles generally validate the approach considered to characterize the DCM, in particular the classification protocol based on analytical forms and the use of parameters issued from their calibration.

A local maximum in BBP profiles can be seen close to the DCM reference depth for most months, considering the notable exception of June (Fig. 9).

The first DCM profiles in March correspond to a well defined maximum in BBP values. From April to June/July, the BBP profiles depict high values in the surface layers, which are not matched by Chla values. This vertical discrepancy in the BBP to Chla ratio may denote 1) the presence of non-phytoplanktonic particles in the upper layers, 2) larger cellular Chla content for phytoplankton located around the DCM, and/or 3) an important difference in terms of phytoplanktonic communities, in particular in terms of cell sizes. For the late DCM period (August-October), a subsurface BBP maximum at the level of the DCM is more systematically visible, although high near-surface BBP values remain.

4 Discussion

4.1 Using BGC-Argo to decipher the Black Sea DCM dynamics

The spatial distribution of BGC-Argo datasets is incomplete and opportunistic. Besides, free-floating floats tend to exclude areas characterized with divergent flow such as the shelf regions or the center of the two central gyres. However, the regular float sampling protocol permits an even seasonal sampling of the central basin, which constitutes an asset compared to traditional datasets, and provides a decent number of observations when considering the monthly perspective adopted in this study (Fig. 3). Furthermore, the dense vertical sampling characterizing Argo datasets permits a refined characterization of DCM depth- and density-diagnostics. BGC-Argo floats thus allow to evidence a clear seasonal DCM dynamics that prevails for the entire central Black Sea, with almost all profiles categorized as DCM from April to September (Fig. 3). During this period the DCM

https://doi.org/10.5194/bg-2020-295
Preprint. Discussion started: 2 September 2020

concentrates 50-70% of the total Chla content in a narrow layer located from 40 to 30 m below the surface, where local PAR conditions reache from 0.5 to 4.5 % of surface incoming radiation.

These depths obtained for the DCM are deeper than those previously reported by Finenko et al. (2005), but the lack of overlapping data prevents to discuss if this should be related to methodological reasons or interannual variability. One could consider, however, the fact that both Yunev et al. (2005) and Finenko et al. (2005) used a single analytical form (modified Gaussian) to characterize Chla distribution as a function of depth during the DCM season. Here, the use of refined analytical forms and subsequent criterion to classify DCM and non-DCM profiles provides a refined description of DCM diagnostics. In particular, to ignore the distinction between DCM and non-DCM profiles may considerably bias the estimates obtained for DCM diagnostics.

As for now, BGC-Argo floats only provide limited proxies to evaluate the relationship between chlorophyll content and phytoplankton biomass, which is essential to upscale the present analysis to larger scale considerations such as productivity and carbon sequestration issues. This might change in the future, however, considering the foreseen enrichment of the Argo's sensor apparatus (e.g. Underwater Vision Profiler (Picheral et al., 2010), with a 6th version to be embedded on future floats). However, the fact that the first DCM profiles (March) correspond to a clear maximum in BBP (Fig. 9) suggests that the DCM is initiated also as a peak in phytoplankton biomass and not only as a local increase in the chlorophyll cellular content, as suggested by Finenko et al. (2005). From April to July, surface maxima in BBP tend to favor the interpretation of DCMs being related to high intra-cellular chlorophyll content, which is in line with the conclusions of Finenko et al. (2005). Here again, the known disparity in species dominance between surface and subsurface waters (Mikaelyan et al., 2020), and in particular regarding the size of dominant species, prevents to consider a strict relationship between particle backscaterring and planktonic biomass. Finally, from August to October, a clear correspondence between Chla and BBP profiles supports the hypothesis that the depicted DCM does indeed correspond to a local peak in planktonic biomass.

4.2 Considering horizontal variability in the depth and density coordinate systems

Both Yunev et al. (2005) and Finenko et al. (2005) consider a depth scale to characterize the vertical distribution of Chla during the DCM period. Yunev et al. (2005) completes this analysis by assessing, for each considered profiles, the depth of the 16.2 $\mathrm{kg\,m^{-3}}$ isopycnal, in order to characterize sub-regions (or "hydrodynamic regimes") of the central Black Sea. The authors conclude that z_{DCM} can be considered as independent from hydrodynamic regimes, which amount to say that depth-diagnostics are sufficiently consistent across the basin to serve as a basis for interannual trends analysis. On the contrary, Finenko et al. (2005) highlight the variability of z_{DCM} and consider it in relation to the surface Chla content, as the author seek to formulate a general relationship allowing to retrieve the vertically integrated biomass from remote sensing surface observations. The authors do not further comment on the spatial structure of DCM diagnostics.

Our results indicate that z_{DCM} indeed presents a substantial variability when considered on a vertical scale, but that this variability is mainly a direct consequence of the spatial variability in the z_{MLD}, and can thus be reduced by considering a density scale. No clear spatial pattern emerges from the analysis of DCM depth-diagnostics, and Fig. 4 highlight that the seasonality of the DCM dynamics is consistent for the entire central basin. The Black Sea can thus be distinguished from the

https://doi.org/10.5194/bg-2020-295
Preprint. Discussion started: 2 September 2020

Mediterranean conditions, in which clear longitudinal gradients in environmental conditions (nutrients and light) induce spatial gradients for DCM characteristics, visible all along the DCM period (Letelier et al., 2004; Mignot et al., 2014; Lavigne et al., 2015).

Nevertheless, the open Black Sea does present a major spatial structure which lies in the general curvature of isopycnals: layers of equal density are dome-shaped and significantly shallower in the center than in the periphery. In addition, isopycnals are subject to vertical motion at time scales of days-weeks under the influence of internal waves, and mesoscale dynamics. This brings many authors to use density as a vertical coordinate system, rather than depth, to minimize the spread of vertical diagnostics and reduced artifacts resulting from unevenly sampled scarce datasets (Tugrul et al., 1992).

Using a density scale thus reduces the horizontal variability of vertical diagnostics characterizing layers that are maintained by diffusion along isopycnals, such as the nitracline and oxycline depths. On the other hand, one might expect that light in-situ conditions, for instance, that proceed from instantaneous vertical penetration would be more homogeneously described on a depth scale. This last assumption, of course, is restricted by the fact that seawater constituents contributing to light attenuation might themselves be distributed along isopycnals. To decipher which driving factors rule the development and structure of DCM dynamics in the Black Sea, we thus consider in the following discussion the spread of the different depth and density horizons presented in Sect. 3.2.1.

The spreads depicted by monthly interquartile ranges and extrema in figures 5 and 6 mainly derive from interannual and/or horizontal variability. Here, we assume that a seasonal change in the spread of some variable (eg. narrow range in spring, large range in autumn) denotes a change in its horizontal variability, since we would not expect interannual variations to be so strictly seasonally consistent (Sect. 4.4 on interannual variability).

4.3 Drivers of the DCM dynamics

All along the season, the lower boundary of the Chla bulk, $z_{50,bottom}$, remains attached to the density layer reached by the winter maximum MLD. The DCM develops from this lower boundary and remains at the same pycnal level until September. During this period, and in particular in August during which the DCM concentrates the biggest part of the Chla content, the spread of DCM location is relatively low on a pycnal scale, and rather large on a depth scale. This indicates that the DCM dynamics is firstly settled by density-structured factors, such as turbulent diffusion, and attached to particular water masses. It then develops until August by remaining attached to these particular water masses, rather than adapting instantaneously to depth-structured factors, such as light, in agreement with the hypothesis formulated by Navarro and Ruiz (2013).

In September and October, surface incoming irradiance decreases, mixing increases and several diagnostics of the Chla vertical distributions migrate upward (both on depth and density scales). During this period, the spreads of Chla diagnostics decrease on a depth scale, while these largely increase on a density scale. According to our frame of analysis, this indicates that, by the end of the DCM season, the DCM is detached from its initial water mass and restructured by depth-related environmental factors. It is worth noting that this transition is first visible for the upper boundary of the Chla bulk content in September, while lower horizons (DCM, lower boundary) remain stable until October.

https://doi.org/10.5194/bg-2020-295
Preprint. Discussion started: 2 September 2020

To further test this analysis, a ratio has been derived between individual σ_{DCM} values and $\sigma_{MLD,max}$, i.e. the maximum σ_{MLD} value experienced by the same float in the same year (Fig. 10a). This ratio is strongly segregated around one in the two first months of the DCM period, regardless of spatial or interannual variability, which clearly indicates that the depth of initial DCM settlement is ruled basin-wide by the intensity of winter mixing.

Both the value and the spread of the ratio remain relatively constant further along the DCM period. In October, last month of the DCM period, and only for the western part of the basin, the ratio decreases and its spread expands largely. This indicates that upon closure of the DCM season, local environmental conditions drive the DCM upwards in ways that are affected by a significant spatial variability.

Light conditions at depth can hardly be considered as an external structuring factor, given that absorption and backscattering by phytoplankton cells induce a direct impact of the DCM on light attenuation. Yet, non-planktonic factors also imprint spatial variability on light attenuation in the Black Sea (Churilova et al., 2017, and references therein), so that light conditions found at the DCM may vary spatially and are worth further investigation.

The DCM is initially set at relatively poor light conditions ($\sim 1\%$ of surface incoming PAR, Fig. 10b). Further along the DCM season, light conditions met at the DCM depth increase globally to reach $\sim 2.2\%$ of surface incoming PAR. This is explained first, by a slight vertical displacement of the DCM from May to June (Fig. 5) and then by the depletion of surface Chla content (see Fig. 7 and appearance of Gaussian profiles in Fig. 3) allowing a deeper light penetration in summer (Fig. 5).

This increase in light at the DCM suggests a gradual positioning of the DCM towards optimal growth conditions. We also note that the longitudinal gradient highlighted in Fig. 10a, is not visible for the light conditions at DCM (Fig. 10b), suggesting indeed that this positioning for light is driven by local conditions. Yet, light conditions at DCM always present a relatively large spread, reaching between 0.5 and 4.5% of the surface incoming PAR at the end of the DCM period. This tends to indicate that other factors limit the DCM potential to seek upward for more light.

The spatial gradient revealed in Fig. 10a depicts a lower ratio (i.e. DCM occupying lighter pycnal levels) in the western part of the basin, where lateral nutrient inputs are enhanced by the proximity of the northwestern shelf system. It can thus be considered that lateral nutrient inputs trigger this spatial disparity of the Black Sea DCM dynamics that only appears in the very last months of the DCM season. This is in agreement with the fact that the nutrient export from the north-western shelf to the open sea has been evaluated to be maximal in October (Grégoire and Beckers, 2004).

Ultimately, model studies would be required to test different hypotheses on driving forces of the DCM dynamics and to compare these to those identified in other parts of the world, considering in particular, the neighboring Mediterranean sea (Terzić et al., 2019). Our analysis nonetheless indicates a clear pycnal structuring of the DCM depth at its formation, that is primarily set by that the intensity of the winter mixing. After this initial settlement, we consider that the DCM acts as a self-preserving structure seeking to optimize growth conditions, by reaching better enlightened depths as far as nutrient inputs permit, and is thus spatially modulated by nutrient lateral fluxes towards the end of the DCM season in October.

https://doi.org/10.5194/bg-2020-295
Preprint. Discussion started: 2 September 2020

4.4 Interannual variability

Analyzing the interannual variability of the DCM seasonal sequence on the basis of the Argo dataset is difficult. First, because the dataset only expands over five years. Second, because sub-setting the data per year gives even more place to the artifacts induced by uneven spatial sampling, the latter being particularly relevant for 2014 ($\approx$ max 10 profiles/month).

Yet, to give a general appreciation of the stability of the DCM seasonal dynamics, Fig. 11 provides the specific annual expressions of the seasonal dynamics illustrated in Figs. 5, 6, 7 and 8.

The most striking features is the relative stability of the DCM seasonal cycle. Although some years do present some noticeable anomalies with respect to the average seasonal cycle, no clear systematic implications could be drawn from this limited dataset. Questioning the drivers of interannual variability of the seasonal DCM dynamics is thus left over for further studies. We redirect the interested reader to such a corresponding recent analysis proposed by Kubryakova and Kubryakov (2020).

5 Conclusions

In this study, we exploit BGC-Argo data (2014–2019, $\approx$ 1000 profiles) to characterize the vertical distribution of Chla in the Black Sea.

First, we highlight the importance of processing raw fluorescence data obtained by BGC-Argo floats to obtain accurate Chla estimates. In particular this involves applying sensor correction such as proposed by Roesler et al. (2017), correction for CDOM fluorescence as proposed by Xing et al. (2017), and non-photochemical quenching as proposed by Xing et al. (2012). While the above procedures are validated on the basis of an HPLC in-situ profile, we advocate that further in-situ HPLC datasets should be consolidated to fine-tune the corrections of BGC-Argo Fluo measurements in the Black Sea.

Then, the retrieved set of Chla data is used to characterize the seasonal changes in the vertical distribution of Chla, and in particular to discuss mechanisms underlying the DCM dynamics.

Our analyses depict a DCM dynamics that dominates the Chla distribution from April to October, consistently over the entire central basin, which agrees with previous descriptions by Yunev et al. (2005); Finenko et al. (2005). Whereas Yunev et al. (2005) considered that depth-diagnostics of the DCM were sufficiently consistent across the basin to infer long term trends from limited sets, the detailed vertical sampling provided by Argo floats and the use of refined analytical forms to distinguish DCM and non-DCM profiles allowed us to demonstrate a substantial spatial variability in DCM diagnostics expressed on a depth scale. We show indeed that during summer the DCM concentrates 50-70 % of the total Chla content in a 10 m layer located between 12 and 50 m below the surface, where local PAR conditions reach from 0.5 to 4.5 % of surface incoming radiation.

This variability in DCM diagnostics may be alleviated by the use of density coordinates, which provide some indications on the processes driving its formation and development. Density-diagnostics reveal that the DCM is strictly initiated at the pycnal level reached by the winter maximum MLD, and remains attached to this layer in a way that is consistent for the entire central basin and all along the DCM season. This supports the hypothesis proposed by Navarro and Ruiz (2013), in which the DCM is depicted as a self-sustaining structure influencing on its surrounding environment, rather than a local maximum adapting

https://doi.org/10.5194/bg-2020-295
Preprint. Discussion started: 2 September 2020


Biogeosciences Discussions Open Access EGU

instantly to external factors. Only towards the end of the thermocline season (October), the disturbed DCM tends to evolve towards optimal growth conditions which are set by local environmental drivers. This finally opens the way for a substantial spatial gradient structured by the enhanced nutrient lateral inputs in the western region.

As for now, the Black Sea BGC-Argo dataset does not allow to establish a strict relationship between Chla and planktonic biomass. Although the DCM is likely to be associated with the increase of the intra-cellular chlorophyll content at depth in summer, the correspondence between (normalized) chlorophyll and backscaterring maxima observed in March, and from August to October indicates that the DCM is also directly associated with peaks in biomass for those parts of the year.

The dynamics highlighted above permits a direct response of the DCM dynamics to the interannual variability in winter mixing conditions, although such interannual responses were relatively low in recent years, as far as the limited BGC-Argo dataset allows to perceive.

This study highlights the importance of considering the DCM dynamics in the assessment of the Black Sea productivity. In order to further the appreciation of its interannual variability, and to strengthens the extrapolation from Chla to actual biomass and productivity, we advocate for a continuous support and enrichment of the Black Sea BGC-Argo fleet both in terms of number of floats and of equipped sensors.

Code and data availability. Processed data and scripts used for the analyses and figures used in this study are uploaded on GitHub and available at the Zenodo repository Ricour and Capet (2020)

Appendix A: FDOM Method

According to the following equation:

$$FChla_{cor} = FChla_{meas} - FChla_{dark} - Slope_{FDOM} \cdot (FDOM_{meas} - FDOM_{dark}) \quad \text{(A1)}$$

where $FChla_{cor}$ is the corrected Chla obtained by removing from the measured Chla ($FChla_{meas}$) the sensor bias ($FChla_{dark}$, dark signal measured in the absence of Chla) and the contribution from CDOM estimated as proportional (coefficient $Slope_{FDOM}$) to the amount of CDOM estimated as the measured CDOM ($FDOM_{meas}$) corrected for the sensor bias ($FDOM_{dark}$). All values are obtained after conversion from Fluo values (in voltage or digital counts) with parameters provided by the manufacturer of each sensor, in $\mathrm{mg\,m^{-3}}$ for Chla and in ppb for CDOM. $Slope_{FDOM}$ represents the ratio between the fluorescence of CDOM measured by a Chla and a CDOM fluorometer. This ratio is assumed to be constant over depth and its units are given in $\mathrm{mg\,m^{-3}\ ppb^{-1}}$.

Below a certain depth, $FChla_{meas}$ should be zero and hence Equation (A1) gives:

$$FChla_{meas} = FChla_{dark} + Slope_{FDOM} \cdot (FDOM_{meas} - FDOM_{dark}) \quad \text{(A2)}$$

That can also be written as:

$$FChla_{meas} = Slope_{FDOM} \cdot FDOM_{meas} + \alpha \quad \text{(A3)}$$

https://doi.org/10.5194/bg-2020-295
Preprint. Discussion started: 2 September 2020

Biogeosciences Discussions Open Access EGU

where $\alpha = FChla_{dark} - Slope_{FDOM} \cdot FDOM_{dark}$.

α is a constant bias that results from factory calibration error. Equation A3 shows that $Slope_{FDOM}$ and α can be retrieved with a linear regression in the depth range where $FChla_{meas}$ is expected to be zero due to the - assumed - absence of Chla. This depth range starts at the Chla minimum down to the bottom of the profile. In all investigated profiles, the Chla minimum is always deeper than the MLD or the DCM during the stratified season and never below 400 m thus the determination of the depth range for the linear regression is easier than in Xing et al. (2017). Once $Slope_{FDOM}$ and α are known, the profile can be corrected according to Equation A1.

Appendix B: Analytical forms of Chla profiles

Chla profiles were fitted with the following analytical forms: a) Sigmoid, $F(z) = \frac{F_{surf}}{1+e^{(Z_{1/2}-z)s}}$ with F_{surf}, the Chla surface concentration, $Z_{1/2}$ the depth at which the Chla concentration is half the Chla concentration at the surface and s the proxy of the sigmoid fit slope at $Z_{1/2}$; b) Exponential, $F(z) = F_{surf}e^{-\frac{ln\ 2}{Z_{1/2}}\cdot z}$; c) Gaussian, $F(z) = F_{max}e^{-\frac{(z-Z_{max})^2}{dz^2}}$ with F_{max}, the maximum Chla value, Z_{max}, the depth of the DCM and dz, the proxy of the Gaussian fit thickness; d) Gaussian-Exponential, $F(z) = F_{surf}e^{-\frac{ln\ 2}{Z_{1/2}}\cdot z} + F_{max}e^{-\frac{(z-Z_{max})^2}{dz^2}}$; e) Gaussian-sigmoid, $F(z) = \frac{F_{surf}}{1+e^{(Z_{1/2}-z)\cdot s}} + F_{max}e^{-\frac{(z-Z_{max})^2}{dz^2}}$

The initial parameters used before the fitting procedure were chosen based on the observed profiles. F_{surf} was chosen to be the mean Chla value in the MLD, $Z_{1/2}$ was chosen as the depth where F_{surf} was divided by 2 or replaced by the MLD if the MLD was deeper than $Z_{1/2}$. Z_max and F_{max} followed their definition while dz and s were initially fixed at, respectively, 5 m and -0.01. In this configuration, the algorithm converged in most cases.

Author contributions. FR, AC and MG conceptualized the research project. FR and AC proceeded to data curation and validation, formal analysis, conducted the investigation, produced the software code and visualizations and wrote the initial draft. MG acquired the funding and overviewed the project administration. AC, FO and MG supervised the execution of this study. All authors contributed to discuss the methodology and to edit and comment the final draft. FO and BD provided resources and supervision for the experimental part.

Competing interests. The authors declare that they have no conflict of interest.

Acknowledgements. FR would like to thank Marin Cornec and Louis Terrats, PhD students at the Villefranche Oceanographic Laboratory for the scripts they provided (NPQ correction and PAR quality control, respectively). FR would also like to thank Snejana Moncheva, director of IO-BAS and the crew of the RV *Akademik* for their conviviality and their help during the cruise. The authors would like to thank Pierre-Marie Poulain for having provided the BGC-ARGO float for deployment. Finally, FR would like to thank Josephine Ras and Céline Dimier for their help with the HPLC analysis. FR, AC, BD and MG are research fellow, postdoctoral, research associate and research director of the Fonds de la Recherche Scientifique - FNRS, respectively.

https://doi.org/10.5194/bg-2020-295
Preprint. Discussion started: 2 September 2020

References

Anderson, G.: Subsurface chlorophyll maximum in the northeast Pacific Ocean, Limnology and Oceanography, 14, 386–391, 1969.

Ardyna, M., Babin, M., Gosselin, M., Devred, E., Bélanger, S., Matsuoka, A., and Tremblay, J.-É.: Parameterization of vertical chlorophyll a in the Arctic Ocean: impact of the subsurface chlorophyll maximum on regional, seasonal, and annual primary production estimates, Biogeosciences, 10, 4383, 2013.

Argo Data Management Team: Argo User's manual V3.3., 2019.

Beckmann, A. and Hense, I.: Beneath the surface: Characteristics of oceanic ecosystems under weak mixing conditions–a theoretical investigation, Progress in Oceanography, 75, 771–796, 2007.

Capet, A., Troupin, C., Carstensen, J., Grégoire, M., and Beckers, J.-M.: Untangling spatial and temporal trends in the variability of the Black Sea Cold Intermediate Layer and mixed Layer Depth using the DIVA detrending procedure, Ocean Dynamics, 64, 315–324, 2014.

Carranza, M. M., Gille, S. T., Franks, P. J., Johnson, K. S., Pinkel, R., and Girton, J. B.: When Mixed Layers Are Not Mixed. Storm-Driven Mixing and Bio-optical Vertical Gradients in Mixed Layers of the Southern Ocean, Journal of Geophysical Research: Oceans, 123, 7264–7289, 2018.

Chiswell, S. M., Calil, P. H. R., and Boyd, P. W.: Spring blooms and annual cycles of phytoplankton: a unified perspective, J. Plankton Res., 37, 500–508, https://doi.org/10.1093/plankt/fbv021, 2015.

Churilova, T., Suslin, V., Krivenko, O., Efimova, T., Moiseeva, N., Mukhanov, V., and Smirnova, L.: Light absorption by phytoplankton in the upper mixed layer of the Black Sea: Seasonality and parametrization, Frontiers in Marine Science, 4, 2017.

Claustre, H., Sciandra, A., and Vaulot, D.: Introduction to the special section bio-optical and biogeochemical conditions in the South East Pacific in late 2004: the BIOSOPE program, Biogeosciences Discussions, 5, 605–640, 2008.

Claustre, H., Antoine, D., Boehme, L., Boss, E., DOrtenzio, F., DAndon, O. F., Guinet, C., Gruber, N., Handegard, N. O., Hood, M., et al.: Guidelines towards an integrated ocean observation system for ecosystems and biogeochemical cycles, 2009.

Coble, P., Gagosian, R., Codispoti, L., Friederich, G., and Christensen, J.: Vertical distribution of dissolved and particulate fluorescence in the Black Sea, Deep-Sea Research, Part A, 38, S985–S1001, 1991.

Cullen, J.: The deep chlorophyll maximum: comparing vertical profiles of chlorophyll a., Canadian Journal of Fisheries and Aquatic Sciences, 39, 791–803, 1982.

Cullen, J.: Subsurface chlorophyll maximum layers: Enduring enigma or mystery solved?, Annual Review of Marine Science, 7, 207–239, 2015.

de Boyer Montégut, C., Madec, G., Fischer, A., Lazar, A., and Iudicone, D.: Mixed layer depth over the global ocean: An examination of profile data and a profile-based climatology, Journal of Geophysical Research C: Oceans, 109, 1–20, 2004.

Dubinsky, Z. and Stambler, N.: Photoacclimation processes in phytoplankton: mechanisms, consequences, and applications, Aquatic Microbial Ecology, 56, 163–176, 2009.

Ediger, D. and Yilmaz, A.: Characteristics of deep chlorophyll maximum in the Northeastern Mediterranean with respect to environmental conditions, Journal of Marine Systems, 9, 291–303, 1996.

Estrada, M., Marrase, C., Latasa, M., Berdalet, E., Delgado, M., and Riera, T.: Variability of deep chlorophyll maximum characteristics in the northwestern Mediterranean, Marine Ecology Progress Series, 92, 289–300, 1993.

Falina, A., Sarafanov, A., Özsoy, E., and Utku Turunçoğlu, U.: Observed basin-wide propagation of Mediterranean water in the Black Sea, J. Geophys. Res. C: Oceans, 122, 3141–3151, https://doi.org/10.1002/2017JC012729, 2017.

https://doi.org/10.5194/bg-2020-295
Preprint. Discussion started: 2 September 2020

Fennel, K. and Boss, E.: Subsurface maxima of phytoplankton and chlorophyll: Steady-state solutions from a simple model, Limnology and Oceanography, 48, 1521–1534, 2003.

Finenko, Z., Churilova, T., and Lee, R.: Dynamics of the vertical distributions of chlorophyll and phytoplankton biomass in the Black Sea, Oceanology, 45, S112–S126, 2005.

Finenko, Z., Suslin, V., and Kovaleva, I.: Seasonal and long-term dynamics of the chlorophyll concentration in the Black Sea according to satellite observations, Oceanology, 54, 596–605, 2014.

Furuya, K.: Subsurface chlorophyll maximum in the tropical and subtropical western Pacific Ocean: Vertical profiles of phytoplankton biomass and its relationship with chlorophylla and particulate organic carbon, Marine Biology, 107, 529–539, 1990.

Grégoire, M. and Beckers, J.-M.: Modeling the nitrogen fluxes in the Black Sea using a 3D coupled hydrodynamical-biogeochemical model: transport versus biogeochemical processes, exchanges across the shelf break and comparison of the shelf and deep sea ecodynamics, 2004.

Huisman, J., van Oostveen, P., and Weissing, F. J.: Species Dynamics in Phytoplankton Blooms: Incomplete Mixing and Competition for Light, Am. Nat., 154, 46–68, https://doi.org/10.1086/303220, 1999.

Huisman, J., Pham Thi, N., Karl, D., and Sommeijer, B.: Reduced mixing generates oscillations and chaos in the oceanic deep chlorophyll maximum, Nature, 439, 322–325, 2006.

IOC, SCOR and IAPSO: The international thermodynamic equation of seawater - 2010 : Calculation and use of thermodynamic properties, Intergovernmental Oceanographic Commission, Manuals and Guides No. 56, UNESCO (English), 196 pp., 2010.

Ivanov, L. I., Beşıktepe, Ş., and Özsoy, E.: The Black Sea Cold Intermediate Layer, in: Sensitivity to Change: Black Sea, Baltic Sea and North Sea, edited by Özsoy, E. and Mikaelyan, A., pp. 253–264, Springer Netherlands, Dordrecht, https://doi.org/10.1007/978-94-011-5758-2_20, 1997.

Kara, A. B., Wallcraft, A. J., and Hurlburt, H. E.: Sea surface temperature sensitivity to water turbidity from simulations of the turbid Black Sea using HYCOM, J. Phys. Oceanogr., 35, 33–54, 2005.

Kara, A. B., Helber, R. W., Boyer, T. P., and Elsner, J. B.: Mixed layer depth in the Aegean, Marmara, Black and Azov Seas: Part I: general features, Journal of Marine Systems, 78, S169–S180, 2009.

Karabashev, G.: Diurnal rhythm and vertical distribution of chlorophyll fluorescence as evidence of bacterial photosynthetic activity in the Black Sea, Ophelia, 40, 229–238, 1995.

Konovalov, S. and Murray, J.: Variations in the chemistry of the Black Sea on a time scale of decades (1960–1995), Journal of Marine Systems, 31, 217–243, 2001.

Konovalov, S. K., Murray, J. W., Luther, G. W., and Tebo, B. M.: Processes controlling the redox budget for the oxic/anoxic water column of the Black Sea, Deep Sea Res. Part 2 Top. Stud. Oceanogr., 53, 1817–1841, https://doi.org/10.1016/j.dsr2.2006.03.013, 2006.

Kopelevich, O. V., Sheberstov, S. V., Yunev, O., Basturk, O., Finenko, Z. Z., Nikonov, S., and Vedernikov, V. I.: Surface chlorophyll in the Black Sea over 1978–1986 derived from satellite and in situ data, J. Mar. Syst., 36, 145–160, https://doi.org/10.1016/S0924-7963(02)00184-7, 2002.

Kubryakova, E. A. and Kubryakov, A. A.: Warmer winter causes deepening and intensification of summer subsurface bloom in the Black Sea: the role of convection and self-shading mechanism, Biogeosci. Discuss., pp. 1–14, https://doi.org/10.5194/bg-2020-210, 2020.

Lavigne, H., D'Ortenzio, F., Ribera D'Alcalà, M., Claustre, H., Sauzède, R., and Gacic, M.: On the vertical distribution of the chlorophyll a concentration in the Mediterranean Sea: A basin-scale and seasonal approach, Biogeosciences, 12, 5021–5039, 2015.

Letelier, R. M., Karl, D. M., Abbott, M. R., and Bidigare, R. R.: Light driven seasonal patterns of chlorophyll and nitrate in the lower euphotic zone of the North Pacific Subtropical Gyre, Limnology and Oceanography, 49, 508–519, 2004.

https://doi.org/10.5194/bg-2020-295
Preprint. Discussion started: 2 September 2020

Macedo, M., Duarte, P., Ferreira, J., Alves, M., and Costa, V.: Analysis of the deep chlorophyll maximum across the Azores Front, Hydrobiologia, 441, 155–172, 2000.

Marra, J.: Analysis of diel variability in chlorophyll fluorescence, Journal of Marine Research, 55, 767–784, 1997.

Mignot, A., Claustre, H., D'Ortenzio, F., Xing, X., Poteau, A., and Ras, J.: From the shape of the vertical profile of in vivo fluorescence to Chlorophyll-a concentration, Biogeosciences, 8, 2391–2406, 2011.

Mignot, A., Claustre, H., Uitz, J., Poteau, A., D'Ortenzio, F., and Xing, X.: Understanding the seasonal dynamics of phytoplankton biomass and the deep chlorophyll maximum in oligotrophic environments: A Bio-Argo float investigation, Global Biogeochemical Cycles, 28, 856–876, 2014.

Mikaelyan, A. S., Chasovnikov, V. K., Kubryakov, A. A., and Stanichny, S. V.: Phenology and drivers of the winter–spring phytoplankton bloom in the open Black Sea: The application of Sverdrup's hypothesis and its refinements, Prog. Oceanogr., 151, 163–176, 2017a.

Mikaelyan, A. S., Shapiro, G. I., Chasovnikov, V. K., Wobus, F., and Zanacchi, M.: Drivers of the autumn phytoplankton development in the open Black Sea, J. Mar. Syst., 174, 1–11, https://doi.org/10.1016/j.jmarsys.2017.05.006, 2017b.

Mikaelyan, A. S., Kubryakov, A. A., Silkin, V. A., Pautova, L. A., and Chasovnikov, V. K.: Regional climate and patterns of phytoplankton annual succession in the open waters of the Black Sea, Deep Sea Res. Part I, 142, 44–57, https://doi.org/10.1016/j.dsr.2018.08.001, 2018.

Mikaelyan, A. S., Mosharov, S. A., Kubryakov, A. A., Pautova, L. A., Fedorov, A., and Chasovnikov, V. K.: The impact of physical processes on taxonomic composition, distribution and growth of phytoplankton in the open Black Sea, J. Mar. Syst., 208, 103 368, https://doi.org/10.1016/j.jmarsys.2020.103368, 2020.

Miladinova, S., Stips, A., Garcia-Gorriz, E., and Macias Moy, D.: Formation and changes of the Black Sea cold intermediate layer, Prog. Oceanogr., 167, 11–23, https://doi.org/10.1016/j.pocean.2018.07.002, 2018.

Moré, J. J.: The Levenberg-Marquardt algorithm: implementation and theory, in: Numerical analysis, pp. 105–116, Springer, 1978.

Murray, J. W., Top, Z., and Özsoy, E.: Hydrographic properties and ventilation of the Black Sea, Deep Sea Research Part A. Oceanographic Research Papers, 38, S663–S689, 1991.

Navarro, G. and Ruiz, J.: Hysteresis conditions the vertical position of deep chlorophyll maximum in the temperate ocean, Global Biogeochemical Cycles, 27, 1013–1022, 2013.

Nelson, N. B. and Siegel, D. A.: The global distribution and dynamics of chromophoric dissolved organic matter, Ann. Rev. Mar. Sci., 5, 447–476, https://doi.org/10.1146/annurev-marine-120710-100751, 2013.

Organelli, E., Bricaud, A., Antoine, D., and Matsuoka, A.: Seasonal dynamics of light absorption by chromophoric dissolved organic matter (CDOM) in the NW Mediterranean Sea (BOUSSOLE site), Deep Sea Res. Part I, 91, 72–85, https://doi.org/10.1016/j.dsr.2014.05.003, 2014.

Organelli, E., Claustre, H., Bricaud, A., Schmechtig, C., Poteau, A., Xing, X., Prieur, L., D'Ortenzio, F., Dall'Olmo, G., and Vellucci, V.: A novel near-real-time quality-control procedure for radiometric profiles measured by bio-argo floats: Protocols and performances, Journal of Atmospheric and Oceanic Technology, 33, 937–951, 2016.

Ostrovskii, A. G. and Zatsepin, A. G.: Intense ventilation of the Black Sea pycnocline due to vertical turbulent exchange in the Rim Current area, Deep Sea Res. Part I, 116, 1–13, https://doi.org/10.1016/j.dsr.2016.07.011, 2016.

Özsoy, E., Di Iorio, D., Gregg, M. C., and Backhaus, J. O.: Mixing in the Bosphorus Strait and the Black Sea continental shelf: observations and a model of the dense water outflow, J. Mar. Syst., 31, 99–135, https://doi.org/10.1016/S0924-7963(01)00049-5, 2001.

https://doi.org/10.5194/bg-2020-295
Preprint. Discussion started: 2 September 2020

Parslow, J. S., Boyd, P. W., Rintoul, S. R., and Griffiths, F. B.: A persistent subsurface chlorophyll maximum in the Interpolar Frontal Zone south of Australia: Seasonal progression and implications for phytoplankton-light-nutrient interactions, Journal of Geophysical Research: Oceans, 106, 31 543–31 557, 2001.

Picheral, M., Guidi, L., Stemmann, L., Karl, D. M., Iddaoud, G., and Gorsky, G.: The Underwater Vision Profiler 5: An advanced instrument for high spatial resolution studies of particle size spectra and zooplankton, Limnology and Oceanography: Methods, 8, 462–473, 2010.

Proctor, C. and Roesler, C.: New insights on obtaining phytoplankton concentration and composition from in situ multispectral Chlorophyll fluorescence, Limnology and Oceanography: Methods, 8, 695–708, 2010.

Ras, J., Claustre, H., and Uitz, J.: Spatial variability of phytoplankton pigment distributions in the Subtropical South Pacific Ocean: Comparison between in situ and predicted data, Biogeosciences, 5, 353–369, 2008.

Richardson, T. L. and Cullen, J. J.: Changes in buoyancy and chemical composition during growth of a coastal marine diatom: ecological and biogeochemical consequences, Marine Ecology Progress Series, pp. 77–90, 1995.

Ricour, F. and Capet, A.: fricour/DCM-Black-Sea-Paper: Release of data and scripts used in the frame of the paper entitled "Dynamics of the Deep Chlorophyll Maximum in the Black Sea as depicted by BGC-Argo floats", https://doi.org/10.5281/zenodo.3966002, https://doi.org/10.5281/zenodo.3966002, 2020.

Roesler, C., Uitz, J., Claustre, H., Boss, E., Xing, X., Organelli, E., Briggs, N., Bricaud, A., Schmechtig, C., Poteau, A., D'Ortenzio, F., Ras, J., Drapeau, S., Haëntjens, N., and Barbieux, M.: Recommendations for obtaining unbiased chlorophyll estimates from in situ chlorophyll fluorometers: A global analysis of WET Labs ECO sensors, Limnology and Oceanography: Methods, 15, 572–585, 2017.

Röttgers, R. and Koch, B.: Spectroscopic detection of a ubiquitous dissolved pigment degradation product in subsurface waters of the global ocean, Biogeosciences, 9, 2585–2596, 2012.

Schmechtig, C., Claustre, H., Poteau, A., and D'Ortenzio, F.: Bio-Argo quality control manual for the Chlorophyll-A concentration, 2018.

Stanev, E. V., Bowman, M. J., Peneva, E. L., and Staneva, J. V.: Control of Black Sea intermediate water mass formation by dynamics and topography: Comparison of numerical simulations, surveys and satellite data, J. Mar. Res., 61, 59–99, https://doi.org/10.1357/002224003321586417, 2003.

Sverdrup, H. U.: On conditions for the vernal blooming of phytoplankton, J. Cons. Int. Explor. Mer, 18, 287–295, 1953.

Terzić, E., Lazzari, P., Organelli, E., Solidoro, C., Salon, S., D'Ortenzio, F., and Conan, P.: Merging bio-optical data from Biogeochemical-Argo floats and models in marine biogeochemistry, Biogeosciences, 16, 2527–2542, https://doi.org/10.5194/bg-16-2527-2019, 2019.

Tugrul, S., Basturk, O., Saydam, C., and Yilmaz, A.: Changes in the hydrochemistry of the Black Sea inferred from water density profiles, Nature, 359, 137, 1992.

Varela, R., Cruzado, A., Tintore, J., and Garcia Ladona, E.: Modelling the deep-chlorophyll maximum: a coupled physical- biological approach, Journal of Marine Research, 50, 441–463, 1992.

Wong, A., Keeley, R., Carval, T., and the Bio Argo Team: Argo Quality Control Manual for CTD and Trajectory Data, 2018.

Xing, X., Morel, A., Claustre, H., Antoine, D., D'Ortenzio, F., Poteau, A., and Mignot, A.: Combined processing and mutual interpretation of radiometry and fluorimetry from autonomous profiling Bio-Argo floats: Chlorophyll a retrieval, Journal of Geophysical Research: Oceans, 116, 2011.

Xing, X., Claustre, H., Blain, S., D'Ortenzio, F., Antoine, D., Ras, J., and Guinet, C.: Quenching correction for in vivo chlorophyll fluorescence acquired by autonomous platforms: A case study with instrumented elephant seals in the Kerguelen region (Southern Ocean), Limnology and Oceanography: Methods, 10, 483–495, 2012.

https://doi.org/10.5194/bg-2020-295
Preprint. Discussion started: 2 September 2020

Xing, X., Claustre, H., Boss, E., Roesler, C., Organelli, E., Poteau, A., Barbieux, M., and D'Ortenzio, F.: Correction of profiles of in-situ chlorophyll fluorometry for the contribution of fluorescence originating from non-algal matter, Limnology and Oceanography: Methods, 15, 80–93, 2017.

675 Yilmaz, A., Ediger, D., Basturk, O., and Tugrul, S.: Phytoplankton fluorescence and deep chlorophyll maxima in the northeastern Mediterranean, Oceanologica Acta, 17, 69–77, 1994.

Yunev, O. A., Moncheva, S., and Carstensen, J.: Long-term variability of vertical chlorophyll a and nitrate profiles in the open Black Sea: eutrophication and climate change, Marine Ecology Progress Series, 294, 95–107, 2005.

https://doi.org/10.5194/bg-2020-295
Preprint. Discussion started: 2 September 2020

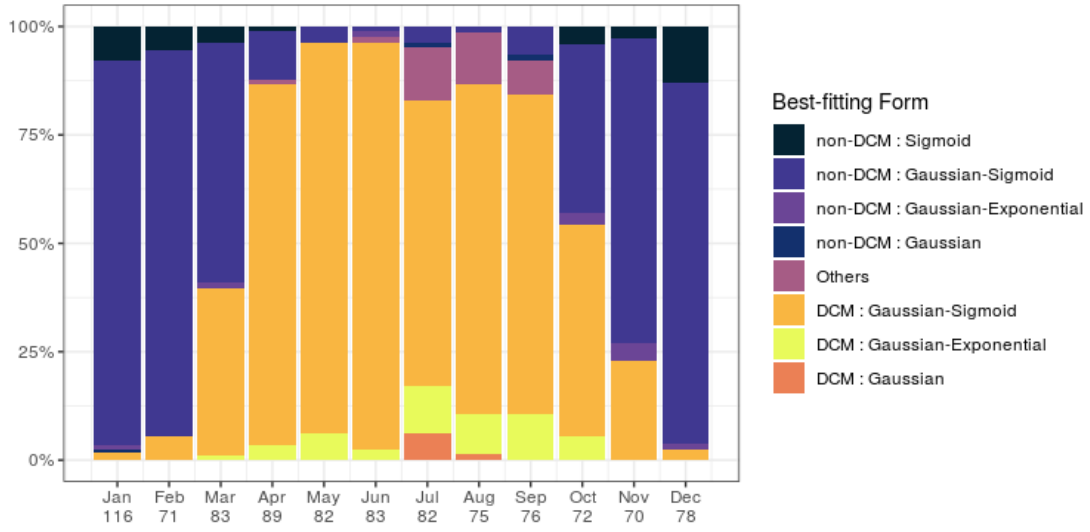

Figure 3. Percentage of best-fitting forms for Chla profiles for each month. Number of profiles are given on the horizontal axis.

https://doi.org/10.5194/bg-2020-295
Preprint. Discussion started: 2 September 2020

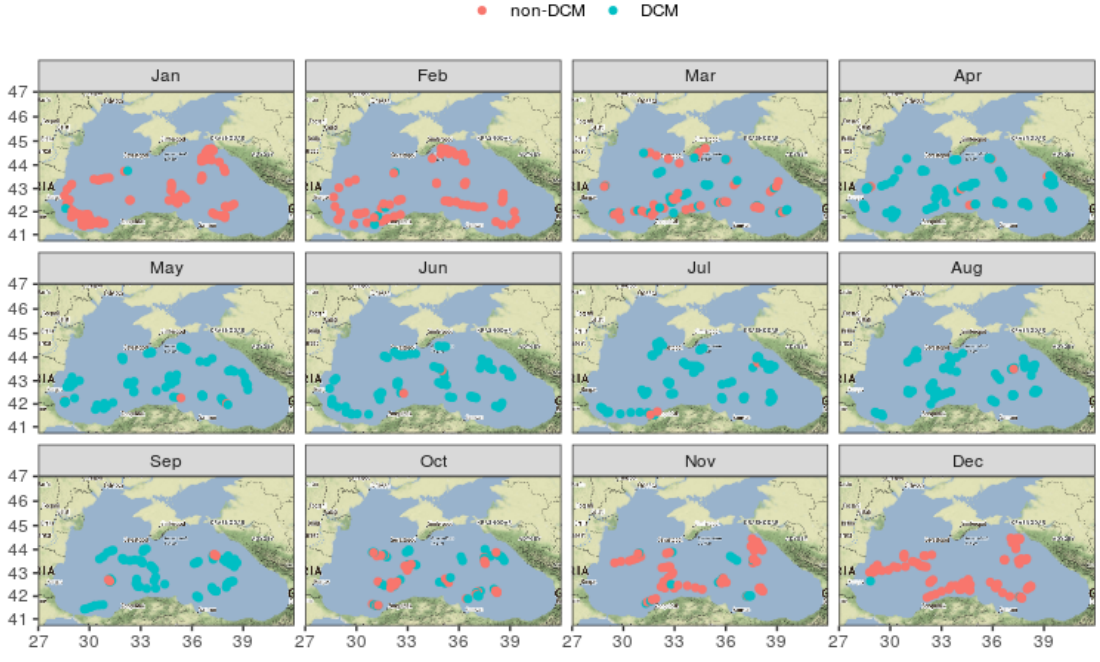

Figure 4. Monthly spatial distribution of DCM and non-DCM profiles indicates homogeneous DCM dynamics in the open basin. This map was created using tiles by Stamen Design, under CC BY 3.0 with data from © OpenStreetMap contributors 2020, distributed under a Creative Commons BY-SA License.

https://doi.org/10.5194/bg-2020-295
Preprint. Discussion started: 2 September 2020

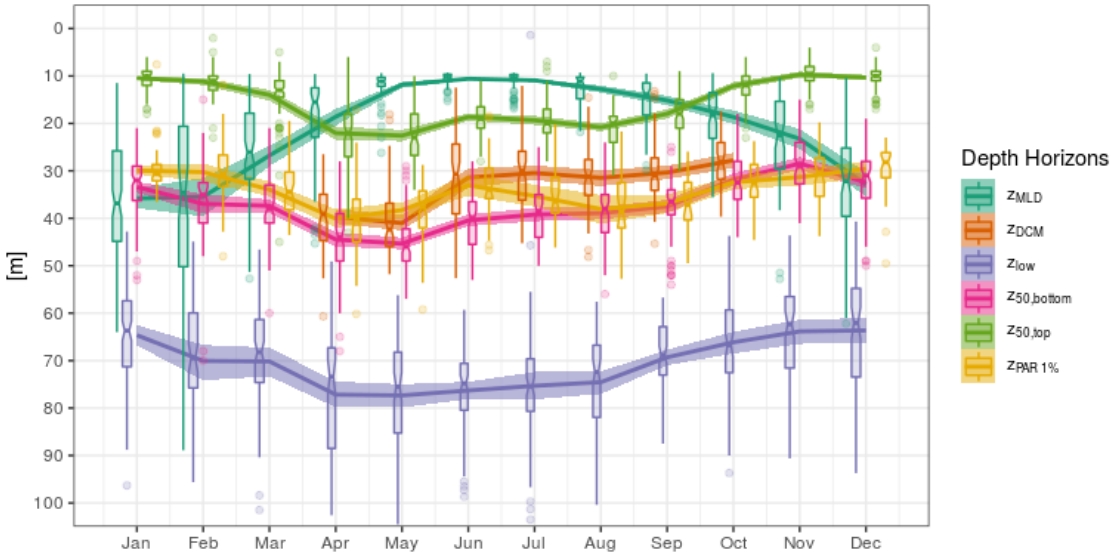

Figure 5. Seasonal variations of depth horizons characterizing the Chla vertical distribution and its environment. Boxplots indicate monthly medians and interquartile ranges. Continuous lines indicate monthly means and their 95% confidence interval (shaded area, bootstrap estimates). While boxplots are slightly shifted to avoid overlapping, the means are all centered on the monthly grid.

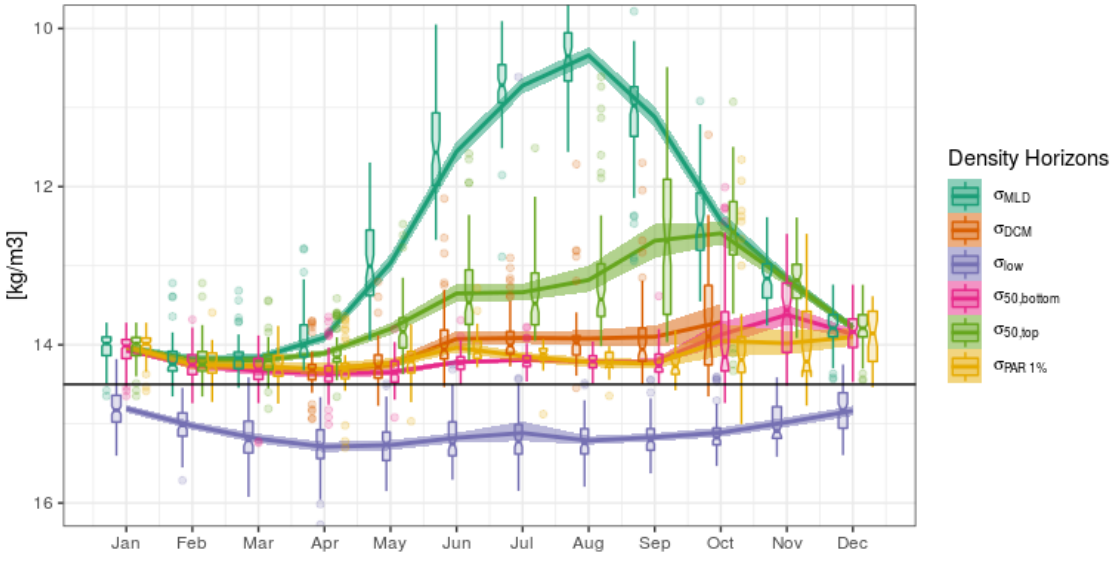

Figure 6. Seasonal variations of density-diagnostics characterizing the Chla vertical distribution and its environment.

https://doi.org/10.5194/bg-2020-295
Preprint. Discussion started: 2 September 2020

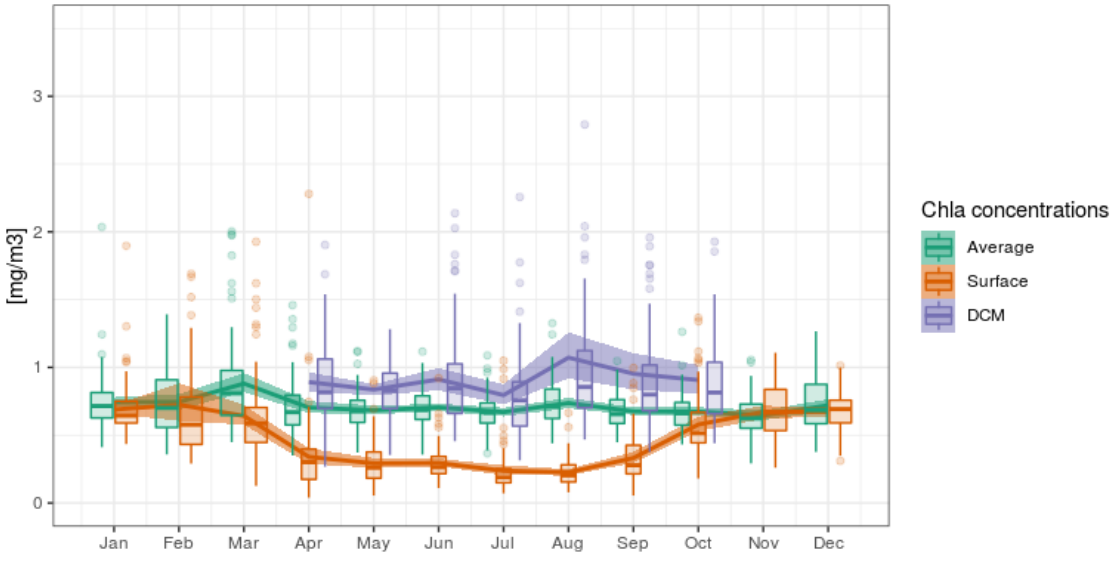

Figure 7. Seasonal variations of surface, DCM and vertically integrated Chla concentrations. Vertically integrated Chla content is scaled by a constant depth of 40 m to reach unit of volumetric concentrations ($\mathrm{mg\,m^{-3}}$).

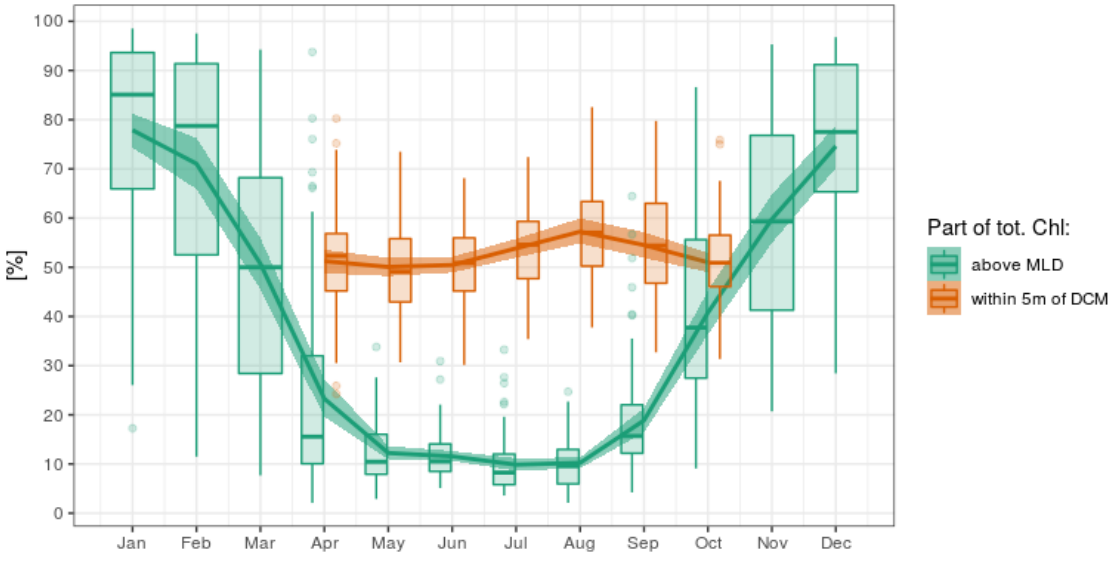

Figure 8. Seasonal variations of relative Chla distribution around specific horizons.

https://doi.org/10.5194/bg-2020-295
Preprint. Discussion started: 2 September 2020

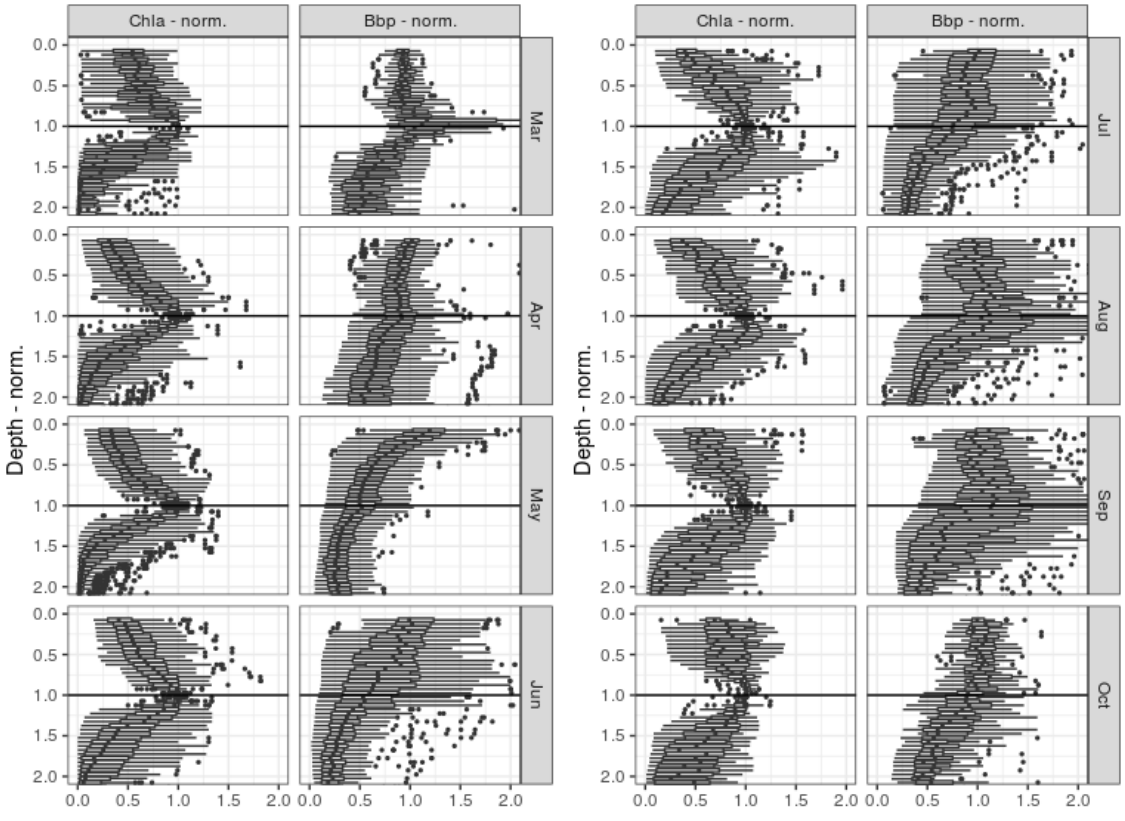

Figure 9. Distribution of normalized Chla and BBP values for different layers of normalized depth (see Sect. 2.6 for the normalization procedure).

https://doi.org/10.5194/bg-2020-295
Preprint. Discussion started: 2 September 2020

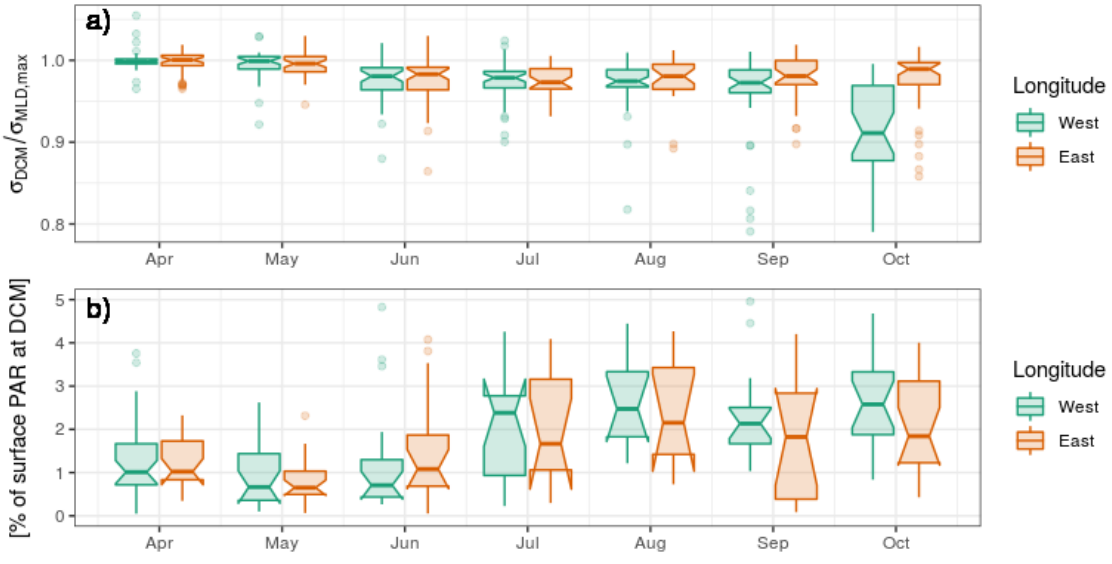

Figure 10. a) Ratio between the σ_{DCM} of individual profiles and the maximum σ_{MLD} recorded by the same float during the same year. b) Fraction of surface incoming PAR that is observed at z_{DCM}. West and East longitude are defined with respect to the meridian of 34.5°E

https://doi.org/10.5194/bg-2020-295
Preprint. Discussion started: 2 September 2020

Figure 11. Interannual variability (year-specific monthly medians) depicted with general monthly seasonal medians, for figures 5 , 6 , 7, and 8.